Frequency-swept feedback interferometry for non-cooperative-target ranging with the stand-off distance of hundred meters

Yifan Wang
Tsinghua University School of Mechanical Engineering https://orcid.org/0000-0001-6927-3638
Xin Xu
Tsinghua University School of Mechanical Engineering
Zongren Dai
Tsinghua University School of Mechanical Engineering
Ziyu Hua
Tsinghua University School of Mechanical Engineering
Chenxiao Lin
Tsinghua University School of Mechanical Engineering
Yubin Hou
Beijing University of Technology Institute of Laser Engineering
Qian Zhang
Beijing University of Technology Institute of Laser Engineering
Pu Wang
Beijing University of Technology Institute of Laser Engineering
Yidong Tan (tanyd@tsinghua.edu.cn)

Research

Keywords: Frequency-swept interferometry, Laser ranging, Laser feedback technique, Remote non-cooperative targets

Posted Date: May 26th, 2022

DOI: https://doi.org/10.21203/rs.3.rs-1655179/v1

Abstract

Frequency-swept interferometry (FSI) is a powerful ranging method with high precision and immunity to ambient light. However, the stand-off distance of the current FSI-based ranging system for non-cooperative targets is relatively short, because the weak echo power cannot provide the needed signal-to-noise ratio (SNR). Here, we report a ranging method combining FSI and the laser feedback technique. Compared with the conventional FSI, the interference between the weak echo signal and the local oscillator occurs in the laser cavity, which makes the signal enhanced spontaneously and then provides a satisfying SNR. In experiments, the detection limit of the echo power is less than 0.1fW, with 230μW output in total. Based on the enhancement from the laser feedback technique, the system achieves a non-cooperative target ranging hundreds of meters away in space without extra optical amplifiers. On the other hand, a large stand-off distance makes the system sensitive to environmental disturbance, which degrades the ranging precision. To correct it, a compensation device is proposed to correct the unwanted optical-path-length drifts. Owing to the high sensitivity and the validity of the compensation, the standard deviation in 10 measurements is better than 0.07mm, targeting an aluminum sheet at about 152m. Generally, hundred-meter range, high relative precision, and low photon consumption predict a novel technical scheme for laser ranging, and demonstrate new capabilities that promise to enable a wide range of scientific and industrial applications.

1. Introduction

The last several decades have witnessed the importance of laser ranging [1–4]. Many industrial, scientific, and military systems seek a reliable, high precision, and non-contact method for distance measurements. Recently, the flourishing developments of automatic driving, 3-D profilometry, and space exploration, have further driven the need for absolute distance measurements [5–9]. A high-performance optical range finder has a wild application prospect.

Among the existing optical methods, frequency-swept interferometry (FSI) is attractive because of its satisfying advantages. Compared with conventional time-of-flight (TOF) technology [10], FSI has an inherent immunity to ambient light through coherent detection, as well as high resolution and precision. Different from optical frequency comb [1], both stability and accuracy in measurements of FSI can be achieved inexpensively. Furthermore, an FSI-based ranging finder can monitor the distance and Doppler-based velocity of the target simultaneously in a single measurement[11, 12]. That is of great significance when monitoring moving targets.

With the above advantages, the FSI-based range finder has become a hotspot since its inception in the 1980s [3]. Recently, many optimizations have been performed for the range finder, in terms of consuming time, precision, measuring range, and stability [13–17]. To date, a 100 kHz-level measuring rate has been realized with micrometers scale resolution [8]. The reliable precision is guaranteed by a more accurate system calibration [18] and a more effective signal analysis algorithm [19, 20]. Additionally, the usage of

silicon photonics chips and embedded digital signal processors makes compatible and real-time measurements possible[21–23].

However, the measured target in most of the optical ranging methods is a corner prism or a reflector. More generally in practice, targets to be monitored cannot reflect enough power, like the surface to be evaluated in manufacturing and the key devices to be positioned in large equipment installations. For these non-cooperative targets, the farthest detectable stand-off distance is greatly shorter and the precision is lower, because the weak echo power cannot provide desirable signal intensity higher than the noise greatly. To strengthen the signal-to-noise ratio (SNR), many efforts have been made [18, 24–26]. A direct way is to increase the probe beam power. High power laser with sub-watt output is selected as the source and optical amplifiers are used for probe beam enhancement. These methods are easy to implement, especially considering the maturity of erbium-doped fiber amplifiers, but the power consumption and system complexity increase in the meanwhile. Other solutions focus on decreasing the detector noise level, such as using an avalanche photodetector (APD) [27]. However, enough echo laser power is also necessary for a desirable SNR in this way, and the usage of high-sensitivity photodetectors increases the costs which limit the applications. In total, the non-cooperative target restricts the ranging system in complexity, power consumption, as well as device costs, and affects the SNR of the detection. Simple structure, high echo signal sensitivity, and low photon consumption are desirable in ranging scenarios, where the limitation of existing methods locates exactly.

Fortunately, laser feedback interferometry (LFI) matches well with the requirements. Laser feedback occurs when the output light partially returns to the resonator, which induces intensity and phase modulation of the laser output [28, 29]. The weak feedback signal (i.e. the echo signal) from targets will participate in the stimulated radiation of the laser, and be enhanced spontaneously. Moreover, combined with the heterodyne modulation technique, the measurement signal can resonate with the relaxation oscillation (RO) of the laser, and then get enhanced further. When the modulating frequency is close to the RO peak, the enhancement factor is up to 10^6 [30, 31]. In this regime, the SNR of the modulation signal is independent of the noise of the photodetector (PD) and only shot-noise limited. The laser source in the LFI works as an emitter, responder, as well as intrinsic amplifier. The remarkable amplification makes it monitor non-cooperative targets effectively and easily, which has been applied in displacement and velocity measuring, tomography, particle detection, and other areas[32–36]. Therefore, the combination of LFI and FSI has great potential in providing a weak echo-signal-detecting configuration without neither an extra external amplifier nor highly sensitive PDs.

In this paper, we propose a laser ranging method based on frequency-swept feedback interferometry (FSFI). With ultra-high sensitivity, the system can respond to the weak echo signal and exhibit satisfying performance in remote non-cooperative-target ranging, where the stand-off distance reaches hundreds of meters with a sub-milliwatt probe beam. Additionally, it is verified in experiments that the long-distance transmission will bring an inevitable phase drift affected by surroundings. Although some methods have been proposed for compensation [14, 37], their performance for remote non-cooperative targets is unsatisfying. To improve it, we demonstrate a quasi-common path compensation method. With this

method, we achieve the relative precision up to 1.3×10^{-6}. Totally, with high echo signal sensitivity, high relative precision, high stability, and low photon consumption, such an overall performance of the FSFI ranging method has potential applications in various scenarios including noncontact surface profiling, fiber-optic sensing, reflectometry, positioning, and tomography.

2. Methods

A. Theoretical Model

Figure 1(a) depicts the configuration of the FSFI-based ranging system. The output beams of a frequency-swept laser are divided into two parts by a beam splitter (BS). One branch is for detection by a PD, while the other one, i.e. the probe beam, illuminates a non-cooperative target. With scattering, only a small part of the incident beam goes back along the same way and returns to the laser cavity. Then, the feedback light interferes with the local oscillator. Since the feedback light experiences an extra delay τ, which is induced by the optical path L_{ex}, a beat signal is generated in the laser cavity. When the optical frequency is swept with time linearly in a single trip, the frequency difference between the local oscillator and the feedback is constant. This beat frequency f_b can be derived as Eq. (1), where B and T are the optical frequency swept bandwidth and period respectively. $\alpha = 2B/T$ denotes the chirp rate. c stands for light speed.

$$f_b = \frac{B}{T/2}\tau = \frac{2\alpha L_{ex}}{c} \tag{1}$$

Different from the conventional FSI-based ranging methods, the FSFI removes the reference arm. Instead, the light field in the cavity functions as the reference, which reduces the system complexity. More importantly, beam mixing inside the cavity strengthens the modulation depth of the beat signal greatly, which makes the system sensitive to the weak echo signals. The weak feedback light will participate in the stimulated radiation of the laser. Like a perturbation, it can break the original dynamic state of inversed populations and photons, and then set up a new one. The state-change of the laser will affect the output intensity significantly, which can be monitored easily by a PD. The intensity response can be described as [31, 38]:

$$\frac{\Delta I\left(f_b\right)}{I} = \sqrt{R_{fb}}G\left(f_b\right)\cos\left(2\pi f_b t - \phi_0 + \Delta\phi_\tau\right) \tag{2}$$

where I is the free-running intensity. R_{fb} is the ratio of feedback power, which is proportional to the effective reflectivity of the target. Φ_0 and $\Delta\Phi_\tau$ represent the initial phase and phase related to the external

cavity length L_{ex}. G is the gain factor compared with the detected intensity directly. The value of G is related to the beat frequency f_b. Particularly, if f_b is close to the RO peak frequency of the laser f_{ro}, the beat will resonate with the RO, which enhances the amplitude of the beat signal remarkably. When they coincide, G gets its maximum. Consequently, the FSFI-based system exhibits ultra-high detection sensitivity for weak signals from non-cooperative targets. By analyzing the frequency spectrum of laser output, we can obtain the enhanced beat frequency f_b, as depicted in Fig. 1(c), and get the distance by Eq. (1).

High sensitivity to weak echo signals makes it possible to monitor the position of non-cooperative targets with further distance. However, a long stand-off distance makes the impacts from environments non-ignorable. Typically, the temperature fluctuation, air disturbance, and unwanted vibration of the target will induce the drift of the optical path length (OPL). As reported in [24], the drift will get the signal peak broadened and deviated, which finally degrades the precision. To correct it, we employ a frequency-shifted laser feedback interferometer for the drift compensation (DC-LFI) to measure the OPL drift in hundreds of meters during the measuring. Moreover, the DC-LFI also employs the advantage of high sensitivity and low photon consumption, which fits well with the remote non-cooperative targets. The validity and performance of remote vibration or displacement monitoring have been reported in our previous research [32, 39]. As shown in Fig. 1(d), the probe beams from FSFI and DC-LFI are combined and propagate in the common path, where the drift affects them both. On the other hand, the signals of two systems can be detected individually, because they are from different sources. Like other heterodyne interferometry, the phase drift of the signal can be demodulated in DC-LFI, which will be used to correct the ranging results in real-time.

B. Experimental Setup

A structural diagram of the proposed ranging finder for non-cooperative targets is shown in Fig. 2(a). An erbium-doped distributed feedback (DFB) single-frequency fiber laser is employed as the frequency-swept source (FSS) because of its compactness in size and large mode-hop free range in tuning. The wavelength it radiates belongs to the telecom band around 1550nm. The continuing advancement of fiber optic components makes the system stable and miniaturized. Frequency swept modulation is achieved by stretching the force-preloaded laser cavity mechanically. As Fig. 2(b) shows, one end of the fiber laser is fixed on the support, and the other one is on a piezoelectric ceramic actuator (PZT, P-601.3SL, PI). The periodical motion of the PZT makes the frequency modulated regularly. The swept bandwidth is 200GHz with a central wavelength of 1552nm. More details of the laser are provided in Supplementary 1 Note 1.

The tunable DFB laser outputs 230μW in the forward direction, and it is divided by a fiber coupler (FC_1) into two parts. One part works as the probe beam, which is collimated by a collimator, coupled out of the fiber into space, and finally illuminates a scattering target after hundreds of meters of propagation. The other part from FC_1 is for detection and analysis. One part is monitored by PD_1 through FC_2, while the other one is used as a source of auxiliary Mach-Zehnder-type fiber interferometer, as marked in Fig. 2(a).

Figure 2(c) depicts the specific configuration of the interference. According to the k-sampling technique [40, 41], the auxiliary interference signal can be used to correct the error caused by the nonlinearity in the frequency sweeping. The optical path difference (OPD) between the two arms is used as standard. Therefore, we place the two arms in a heat insulation box (HIB) to prevent the impact of ambient temperature fluctuations. The outputs of the auxiliary interferometer are detected by a balanced photodetector (BPD). Note that two optical isolators (ISOs) are inserted to guarantee the unidirectional propagations of non-probe beams and avoid parasitic optical feedbacks [42]. The parasitic feedbacks are generated by the reflective light from the interfaces of fiber optic devices and pigtails. If without ISOs, each of them will generate a signal peak in the frequency spectrum, which may obstruct the correct peak searching in signal analysis.

Additionally, a DC-LFI is set up to compensate for the impacts of the optical path drift in transmission. We use a solid-state microchip as the source with the fundamental transverse mode and single longitudinal mode. The wavelength is measured at 1064 nm. Collimated by a lens (L_1), the output is divided by a beam splitter into two parts, which are for detection and measurement respectively. The reflective part is monitored by PD_2, and the transmissive part is modulated by a pair of acoustic-optic modulators (AOMs) with central frequencies 70MHz and 71MHz respectively. Selecting the specific diffractive beams, AOMs can provide a differential frequency, f_{AOM}=1MHz in a single transmission and 2MHz in a round-trip. See Supplementary 1 Note 2 for more details about diffraction beam selections. The frequency-shifted beam is collimated by L2 and L3, with the focal length of -25mm and 250mm, to suppress the divergence. Then the probe beam is reflected by a mirror and combined with the probe from FSFI through a dichroic mirror (DM), after which the two beams propagate in the common path to the target. With this compensation device, the phase drift can be monitored and the stand-off distance can be obtained precisely.

Figure 2(d) shows the data acquisition of the system. A symmetry triangle wave is generated by an arbitrary waveform generator (AWG) and drives the PZT for frequency swept. A TTL signal synchronized with the triangle wave functions as the trigger of the data acquisition card (DAQ). The DAQ records data in four channels. Two channels are for FSFI and auxiliary interferometer, which correspond to PD_1 and BPD respectively. The other two are for DC-LFI, monitoring the phase drift of the beam in transmission, which are demodulated by a lock-in amplifier (LIA). The reference signal of LIA is generated by the differential driving signals of AOMs, f_{AOM}, and the input is the detected signal from PD_2. Then, the real part, x, and the imaginary part, y, of the modulated signal are obtained and recorded by DAQ. Finally, the data is transmitted to a computer and analyzed in the frequency domain. Note that a high-pass filter (HPF) is inserted in the auxiliary signal channel. Considering the source of the auxiliary interferometer is the same laser as the ranging module, the auxiliary signal contains the frequency components of ranging. However, the optical path of the delay line is always twice longer than the stand-off distance, according to the Nyquist criterion in resampling. The auxiliary and ranging signals can be separated in the frequency domain, where the HPF filters the ranging signal. More details about the signal process are listed in Supplementary 1 Note 3.

3. Results

We set the output surface of the collimator as the zero point in ranging. Then the stand-off distance R_{mea} can be expressed as:

$$R_{mea} = \frac{L_{ex} - L_f}{n}$$

3

where L_f stands for the OPL in fiber and n for the refractive index. A series of experiments are performed to verify the validity for ranging noncooperative targets.

A. Effectiveness of Compensation

The performance of the compensation method based on DC-LFI is evaluated first. To simulate the unwanted OPL drift in propagation, we use a vibrating aluminum sheet as the ranging target, the effective reflectivity of which is 10^{-7}, calibrated in experiments with a Φ42.5mm collecting aperture. The sheet is attached to another piece of PZT actuator (CoreMorrow, Inc. XMT 150), and placed 9.6 meters away from the collimator of the system. A power amplifier (Aigtek, ATA-4051) drives the sinusoidal vibration of PZT as well as the target, and the amplitude is 2μm. Figure 3(a) lists the ranging results with or without compensation under various frequencies from 1Hz to 1kHz, and the details can be seen in the right column. High-frequency components of the OPL vibration make the bandwidth of the signal broadened obviously, which leads to measurement error. Contrarily, with compensation, the signal peaks can be recognized easily, but also with identical linewidth and peak positions. The proposed method is effective for the unwanted OPL drift from Hz to kHz-scale, which covers the frequency band of environment noise in most cases.

Another experiment is performed to test the validity in remote target ranging. The target is 162.2m away from the system. Figure 3(b) shows the results of ranging in comparison, and Fig. 3(c) is the corresponding OPL drift recorded by DC-LFI during measuring, caused by the environmental factors. The compensated signal peak, with higher SNR and narrower bandwidth, confirms the effectiveness of our method for OPL drift compensation.

B. Precision and Linearity

To evaluate the precision of the system, repeated measurements are conducted with OPL drift compensation. The target is the aluminum sheet mentioned above, and it is fixed on a displacement stage (PI, Inc. M511), 152.76m away from the collimator. The measurements are repeated 10 times, and the standard deviation is calculated. Then, the stage, as well as the target, moves 500μm in each step and 5mm in total. In each position, similar tests are performed. The total data are displayed in Fig. 4(a)., where the experimental data indicates the step motion clearly. Meanwhile, the standard deviation of 10

measurements in 10 positions is also analyzed respectively. They all possess a standard deviation, σ, no more than 0.067mm, corresponding to 1.3×10^{-6} relative precision, calculated by $3\sigma/R_{mea}$.

The linearity test of the system is also carried out, which demonstrates the nonlinear error in measurements. The precision of the stage is 50nm, which can be taken as the standard. The stage drives the aluminum sheet forward by 10 cm, covering the whole travel range of the stage. Meanwhile, the ranging results from the FSFI are recorded. The acquired data, linearly fitting, and residual error are marked in Fig. 4(b). The maximum residual error is 83μm, corresponding to 8.3×10^{-4} linearity within 10 cm at 152.76m.

C. Resolution

In most previous research, the resolution of the ranging system refers to the ability to distinguish between several simultaneously present targets [3], and it is quantified as the full width at half maximum (FWHM) of the signal peak. The resolution, $\Delta R = c/2B$ in theory, is determined by the frequency swept bandwidth B. Similar tests are performed in our system. The aluminum sheet works as the non-cooperative target, and stands 152m away. The signal peak is plotted in Fig. 5(a). Numerically, the FWHM is 0.94 mm, slightly worse than the theory, 0.75mm with 200GHz tuning. This deviation originates mainly from the fiber dispersion of the delay line in the auxiliary interferometer.

Besides, we evaluate the actual resolution of the system, ranging two targets at different distances at the same time. As Fig. 5(b) shows, the probe beam illuminates the aluminum sheet and its iron support. The thickness of the sheet provides a distance difference. The ranging result is illustrated in Fig. 5 (c), where the two-peak signal is recognizable, and the resolution is realized in a real sense. In Fig. 5(d), the gap value fluctuates within 87μm in 10 times repetitions, and the average is 1.076 mm. The system resolves two non-cooperative targets, even after hundreds of meters of propagation, and the experimental resolution is better than 1.1mm.

D. SNR

By Eq. (1), the beat signal can be amplified in the laser cavity. On the other hand, in the band of the significant amplification, the laser intensity (LI) noise also increases remarkably, which is manifested as the RO peak. Additionally, the PD noise is another important source, contributing to the total noise. The normalized power spectra in dB of the signal and noise versus the beat frequency are shown in Fig. 6 (a). The analysis of the SNR is conducted in two cases. (1) In the absence of PD noise, the SNR of FSFI is independent of the beat frequency and only shot-noise limited [31], which can be expressed as:

$$SNR_{FSFI} = \frac{PR_{fb}}{2h\nu\Delta F}$$

4

where P and ΔF represent the laser output power and demodulation bandwidth. v is the frequency of the laser, and it can be approximated as the central frequency of sweeping. h is Planck's constant. (2) With the PD noise, presumed to be white noise, the SNR can also reach shot-noise limitation within a frequency range close to the RO frequency, where the intensity of RO is several orders stronger than the PD noise. In this frequency band, the PD noise will not affect the SNR, even if it is much stronger than the shot noise. The SNR of the beat signal with and without the PD noise is shown in Fig. 6 (b). Due to the enhancement, the system gets rid of the limitation of PD noise in the LN noise-dominating band. Beyond the band, the SNR is also enhanced, merely smaller in value. Totally, the system exhibits ultra-high detection sensitivity and satisfying SNR for weak echo signals, even with low probe-beam power.

In our system, the noise equivalent power (NEP) of PD is 69.5pW/Hz$^{1/2}$, which is tested in experiments. The beam power received by PD is 22μW, which corresponds to 2.3pW/Hz$^{1/2}$ shot noise [43]. Compared with the PD noise, shot noise hardly contributes to the total noise. In the frequency band close to the RO peak, the LI noise is dominant, up to several nW/Hz$^{1/2}$. According to the theory above, when the beat frequency f_b is located in this band, it gets remarkable amplification and provides a satisfying SNR. We evaluate the minimum detected feedback power in this regime. A cube mirror is used as the target to calibrate the power attenuation. An adjustable attenuator is installed before the collimator, which can change the optical attenuation of the probe beam. The demodulation bandwidth ΔF is 17Hz. The SNR-attenuation curve is shown in Fig. 6 (c). The slope of the fitting is 1.027, which verifies the linear relationship in Eq. (4). Meanwhile, the fitting results predict the ideal detection limit (i.e. SNR = 1) is -127.33dB. The output power of the laser is 230μW, corresponding to the minimum echo power of 0.0425fW. The theoretical detection limit is -137.22dB corresponding to 0.0043fW, calculated by Eq. (4). The results from experiments are comparable with the theory, considering the experimental loss, like mode mismatch between the feedback beam and local oscillator.

It is verified that the proposed ranging system exhibits high sensitivity to echo signals with sub-milliwatt output power. This performance demonstrates the system has the potential in ranging non-cooperative targets farther. Figure 6(d) provides the results of ranging with a 460m stand-off distance. An iron block is selected as the target, with 8.3×10^{-7} effective reflectivity under a Φ42.5mm collecting aperture. The signal peak is obvious compared with the noise baseline, and the SNR is over 20dB.

E. Comparison with Conventional FSI-based Ranging system

To have a clear comparison with a conventional FSI-based ranging system (i.e. without optical feedback), we perform another experiment. An FSFI-based and a conventional FSI-based system are set up, and they target the same object under identical conditions, where they employ the same laser source, collimator, auxiliary interferometer, detector, and measure with equal probe beam power. More details of the setup are demonstrated in Supplementary 1 Note 4. The red and black solid lines stand for the PD noise and LI noise respectively, and the LI noise is stronger than the PD noise. The power spectra of the ranging signals are shown in Fig. 7(a)-(b). The SNR of the conventional ranging system is 8.8dB, while the FSFI-

based is 39.4dB. The over 10^3 SNR enhancement verifies the high echo-signal sensitivity of the proposed system when the beat frequency f_b is within the LI-noise dominating frequency band.

Additionally, another experiment is performed when f_b is out of the LI-noise dominating band. We replace another PD with higher NEP, where the PD noise is dominant. The power spectra of two systems in Fig. 7(c)-(d). In this case, the beat signal f_b in the conventional system is submerged in the noise, while the SNR is 25.2dB in the FSFI-based system. The results show the FSFI also exhibits better SNR than conventional LFI in the detector-noise dominating band.

4. Discussion

With low probe-beam power and no extra amplifier, the proposed FSFI-based ranging system achieves the stand-off-distance extension to hundreds of meters in space for non-cooperative-target ranging. Additionally, the ambient impacts have been compensated, which makes our system has a satisfying relative precision. The performance of the system is listed in Table 1.

The farthest stand-off distance is decided by the minimum detectable echo power. In conventional FSI-based ranging, systems all the noise will contribute to the degradation of SNR, typically the PD noise and LI noise. Instead, in the FSFI-based system, the resonance between the RO and the beat signal gets the SNR independent of the PD noise. Equivalently, the PD noise is suppressed remarkably, when the LI noise is comparable with or stronger than the PD noise. Therefore, FSFI works as a general detector-noise eraser, and it makes weak signals detected easily. By Eq. (1), the beat frequency f_b is proportional to the product of stand-off distance L_{ex} and chirp rate a. To obtain a merely shot-noise-limited SNR, adjusting the chirp rate

Table 1
Characteristics of the proposed FSFI-based ranging system

Parameter	Value
Central wavelength of sweeping	1552 nm
Output power	230μW
Minimum detectable echo power	0.043fW
Swept bandwidth	200GHz
Stand-off distance	Hundreds of meters
Precision	3σ = 0.2 mm @152m
Relative Precision	1.3×10^{-6}
Actual resolution	1.1mm
Sweeping Frequency	~ 10Hz

moderately is necessary for a feasible beat frequency. Additionally, adding extra optical amplifiers, a common improvement in conventional methods, is also compatible with FSFI, which can be used to enhance the SNR and extend the stand-off distance further.

The main factor affecting the precision is the variation of OPD between two arms in the auxiliary interferometer. According to the k-sampling technique, the length of OPD is regarded as the standard in ranging and should be longer than the desired maximum measurement distance by the Nyquist criterion. Since the stand-off distance in this paper exceeds 100m, the OPD of the auxiliary interferometer is over 400m. In experiments, the length of OPD is calibrated by a gas absorber cell (Wavelength References HCN-13-H(5.5)-25-FCAPC) initially. However, it is hard to keep the OPD constant during measurements because of the environment-condition changes. For example, considering the thermal expansion, the OPD variation is up to 3.4mm/$^{\circ}$C. Although we use a heat insulation box to prevent the disturbance from environments, the temperature fluctuation induced OPD drift is in tens of micrometers scale. If higher precision is required, the auxiliary interferometer should be optimized or replaced by other nonlinearity correction methods including phased locked loop, frequency comb calibration [18], and digital pre-distortion [44].

The resolution is determined by the frequency-swept bandwidth and limited by the travel range of the PZT specifically in our system. Large tuning bandwidth demands large stretching of the DFB fiber laser cavity and correspondingly a large driving force of PZT. A more powerful PZT actuator or other tunable intracavity devices, such as a Fabry-Perot filter [45], can improve the resolution. In addition, the dispersion of the delay line also extends the signal peak and get the resolution decreased. This extension is proportional to the frequency swept bandwidth. Compared with other systems, the bandwidth in our system is relatively small. Therefore, the dispersion-induced bandwidth increment is neglected compared with the intrinsic FWHM, ΔR. More analysis of dispersion is demonstrated in Supplementary 1 Note 5.

Another limitation of the system is the time consumption, which relates to the realization of real-time measurements. Currently, the sweeping frequency determines the measuring rates. The resonant frequency of the PZT is 322Hz. To avoid device damage, the frequency of the triangular wave is less than 100Hz. Overall considered, the swept frequency of the system is less than 60Hz. Consequently, the usage of mechanical modulation in our system, makes the rate much slower than electrical modulation for laser diode (LD). However, in the LD-based FSFI system, the sensitivity to echo signals is inferior to the solid-state laser [46]. The trade-off is governed by demands in specific applications.

On the other hand, the data processing time is another consumption. In each measurement, a few frequency components have the sample information, and others are nearly zero. Considering the size and sparsity of the data, using sparse FFT can get the process efficiently. Other compressed sensing methods may also be used in the future. Besides, the processing is implemented in MATLAB. Rewriting the processing code in C/C++, together with GPU-accelerated parallel processing, can significantly reduce the processing time.

5. Conclusions

In conclusion, an FSFI-based laser ranging system is developed. Owing to the laser feedback configuration, the ranging signal will resonate with the RO and then get enhanced spontaneously. In this regime, the significant enhancement provides a satisfying SNR, and makes remote non-cooperative-target ranging possible. In experiments, the stand-off distance is up to hundreds of meters, while the probe beam power is in sub-milliwatt level. The high sensitivity of the laser feedback technique is also employed in the OPL-drift compensation to improve the precision of ranging. The performance tests demonstrate the necessity and validity of the compensation. With it, the system exhibits a precision better than 0.2mm and actual resolution better than 1.1mm. Compared with the conventional FSI-based system, the advantages of the proposed one can be summarized as high echo signal sensitivity, high relative precision, a large range of ranging, and lower photon consumption. These features provide an extra solution to remote-target ranging. Although a lot to be improved including resolution and measuring rate, the optimized sensor promises a wider prospect in scientific and industrial applications including 3-D profilometry, positioning, and space exploration.

Abbreviations

FSI
Frequency-swept interferometry
SNR
Signal-to-noise ratio
TOF
Time-of-flight
APD
Avalanche photodetector
LFI
Laser feedback interferometry
RO, Relaxation osculation
PD
photodetector
FSFI
Frequency-swept feedback interferometry
BS
Beam splitter
OPL
Optical path length
DC-LFI
Laser feedback interferometer for the drift compensation. DFB:Distributed feedback
FSS

Frequency-swept source
PZT
Piezoelectric ceramic actuator
FC
fiber coupler
OPD
Optical path difference
HIB
Heat insulation box
BPD
Balanced photodetector
ISO
Isolator
L, Lens
AOM
Acoustic-optic modulator
DM
Dichroic mirror
AWG
Arbitrary waveform generator
DAQ
Data acquisition card
LIA
Lock-in amplifier
HPF
High-pass filter
FWHM
Full width at half maximum
LI, laser intensity
NEP
Noise equivalent power
LD
laser diode.

Declarations

Acknowledgments

The authors gratefully acknowledge the team of Prof. F Zhang from Tianjin University and the team of Prof. G Liu from Harbin Institute of Technology for technical support.

Authors' contributions

YW and YT proposed the framework of this research. YH, QZ, and PW designed and fabricated the key device. YW, XX, ZD, and ZH conducted the experiments. YW and CL carried out the data processing. All the authors participated in the result analysis and discussion, and contributed to the writing of the manuscript.

Funding

National Science Fund for Distinguished Young Scholars (51722506); Tsinghua University Initiative Scientific Research Program (2021Z11GHX002); Shunde Core Technology Research Program (2130218003012).

Availability of data and materials

The datasets used and analysed during the current study are available from the corresponding author on reasonable request.

Declarations

Ethics approval and consent to participate

There is no ethics issue for this paper.

Consent for publication

All authors agreed to publish this paper.

Competing interests

The authors declare that they have no competing interests.

References

1. Coddington I, Swann WC, Nenadovic L, Newbury NR. Rapid and precise absolute distance measurements at long range. Nature Photonics. 2009;3(6):351-6. doi: 10.1038/nphoton.2009.94.
2. Lu F, Milios E. Robot pose estimation in unknown environments by matching 2D range scans. Journal of Intelligent & Robotic Systems. 1997;18(3):249 – 75. doi: 10.1023/a:1007957421070.
3. Uttam D, Culshaw B. Precision time domain reflectometry in optical fiber systems using a frequency modulated continuous wave ranging technique. Journal of Lightwave Technology. 1985;3(5):971-7. doi: 10.1109/jlt.1985.1074315.
4. Trocha P, Kemal JN, Gaimard Q, Aubin G, Lelarge F, Ramdane A, et al. Ultra-fast optical ranging using quantum-dash mode-locked laser diodes. Sci Rep. 2022;12(1):1076. doi: 10.1038/s41598-021-04368-4.

5. Mitchell EW, Hoehler MS, Giorgetta FR, Hayden T, Rieker GB, Newbury NR, et al. Coherent laser ranging for precision imaging through flames. Optica. 2018;5(8). doi: 10.1364/optica.5.000988.
6. Levinson J, Askeland J, Becker J, Dolson J, Held D, Kammel S, et al. Towards Fully Autonomous Driving: Systems and Algorithms. IEEE Intelligent Vehicles Symposium (IV). Baden-Baden, GERMANY2011. p. 163-8.
7. Steindorfer MA, Kirchner G, Koidl F, Wang P, Jilete B, Flohrer T. Daylight space debris laser ranging. Nat Commun. 2020;11(1):3735. doi: 10.1038/s41467-020-17332-z.
8. Wang Z, Potsaid B, Chen L, Doerr C, Lee HC, Nielson T, et al. Cubic meter volume optical coherence tomography. Optica. 2016;3(12):1496 – 503. doi: 10.1364/OPTICA.3.001496.
9. Ula RK, Noguchi Y, Iiyama K. Three-Dimensional Object Profiling Using Highly Accurate FMCW Optical Ranging System. Journal of Lightwave Technology. 2019;37(15):3826-33. doi: 10.1109/jlt.2019.2921353.
10. Lee J, Kim Y-J, Lee K, Lee S, Kim S-W. Time-of-flight measurement with femtosecond light pulses. Nature Photonics. 2010;4(10):716 – 20. doi: 10.1038/nphoton.2010.175.
11. Martin A, Verheyen P, De Heyn P, Absil P, Feneyrou P, Bourderionnet J, et al. Photonic Integrated Circuit-Based FMCW Coherent LiDAR. Journal of Lightwave Technology. 2018;36(19):4640-5. doi: 10.1109/jlt.2018.2840223.
12. Dong Y, Zhu Z, Tian X, Qiu L, Ba D. Frequency-Modulated Continuous-Wave LIDAR and 3D Imaging by Using Linear Frequency Modulation Based on Injection Locking. Journal of Lightwave Technology. 2021;39(8):2275-80. doi: 10.1109/jlt.2021.3050772.
13. Hauser M, Hofbauer M. FPGA-Based EO-PLL With Repetitive Control for Highly Linear Laser Frequency Tuning in FMCW LIDAR Applications. IEEE Photonics Journal. 2022;14(1):1–8. doi: 10.1109/jphot.2021.3139053.
14. Zhang F-M, Li Y-T, Pan H, Shi C-Z, Qu X-H. Vibration Compensation of the Frequency-Scanning-Interferometry-Based Absolute Ranging System. Applied Sciences. 2019;9(1). doi: 10.3390/app9010147.
15. Cheng X, Liu J, Jia L, Zhang F, Qu X. Precision and repeatability improvement in frequency-modulated continuous-wave velocity measurement based on the splitting of beat frequency signals. Opt Express. 2021;29(18):28582-96. doi: 10.1364/OE.433637.
16. Li B, Mo D, Wang P, Gan N, Lin M, Wang R, et al. FMCW lidar multitarget detection based on skeleton tree waveform matching. Appl Opt. 2021;60(27):8328-35. doi: 10.1364/AO.431516.
17. Pan H, Qu X, Zhang F. Micron-precision measurement using a combined frequency-modulated continuous wave ladar autofocusing system at 60 meters standoff distance. Optics Express. 2018;26(12):15186-98. doi: 10.1364/oe.26.015186.
18. Baumann E, Giorgetta FR, Deschenes JD, Swann WC, Coddington I, Newbury NR. Comb-calibrated laser ranging for three-dimensional surface profiling with micrometer-level precision at a distance. Opt Express. 2014;22(21):24914-28. doi: 10.1364/OE.22.024914.

19. Hao Y, Song P, Wang X, Pan Z. A Spectrum Correction Algorithm Based on Beat Signal of FMCW Laser Ranging System. Sensors (Basel). 2021;21(15). doi: 10.3390/s21155057.
20. Okano M, Chong C. Swept Source Lidar: simultaneous FMCW ranging and nonmechanical beam steering with a wideband swept source. Opt Express. 2020;28(16):23898-915. doi: 10.1364/OE.396707.
21. Norgia M, Melchionni D, Pesatori A. Self-mixing instrument for simultaneous distance and speed measurement. Optics and Lasers in Engineering. 2017;99:31 – 8. doi: 10.1016/j.optlaseng.2016.10.013.
22. Zhang X, Kwon K, Henriksson J, Luo J, Wu MC. A large-scale microelectromechanical-systems-based silicon photonics LiDAR. Nature. 2022;603(7900):253-8. doi: 10.1038/s41586-022-04415-8.
23. Norgia M, Magnani A, Pesatori A. High resolution self-mixing laser rangefinder. Rev Sci Instrum. 2012;83(4):045113. doi: 10.1063/1.3703311.
24. Lu C, Xiang Y, Gan Y, Liu B, Chen F, Liu X, et al. FSI-based non-cooperative target absolute distance measurement method using PLL correction for the influence of a nonlinear clock. Opt Lett. 2018;43(9):2098 – 101. doi: 10.1364/OL.43.002098.
25. Mateo AB, Barber ZW. Multi-dimensional, non-contact metrology using trilateration and high resolution FMCW ladar. Appl Opt. 2015;54(19):5911-6. doi: 10.1364/AO.54.005911.
26. Zhang K, Lv T, Mo D, Wang N, Wang R, Wu Y. Double sideband frequency scanning interferometry for distance measurement in the outdoor environment. Optics Communications. 2018;425:176-9. doi: 10.1016/j.optcom.2018.04.056.
27. Ahmad Z, Liao Y-M, Kuo S-I, Chang Y-C, Chao R-L, Naseem, et al. High-Power and High-Responsivity Avalanche Photodiodes for Self-Heterodyne FMCW Lidar System Applications. IEEE Access. 2021;9:85661-71. doi: 10.1109/access.2021.3089082.
28. Taimre T, Nikolic M, Bertling K, Lim YL, Bosch T, Rakic AD. Laser feedback interferometry: a tutorial on the self-mixing effect for coherent sensing. Advances in Optics and Photonics. 2015;7(3):570–631. doi: 10.1364/aop.7.000570.
29. Giuliani G, Norgia M, Donati S, Bosch T. Laser diode self-mixing technique for sensing applications. Journal of Optics a-Pure and Applied Optics. 2002;4(6):S283-S94. doi: 10.1088/1464-4258/4/6/371.
30. Otsuka K. Self-mixing thin-slice solid-state laser Doppler velocimetry with much less than one feedback photon per Doppler cycle. Optics Letters. 2015;40(20):4603-6. doi: 10.1364/ol.40.004603.
31. Lacot E, Day R, Stoeckel F. Coherent laser detection by frequency-shifted optical feedback. Physical Review A. 2001;64(4). doi: 10.1103/PhysRevA.64.043815.
32. Zhu K, Guo B, Lu Y, Zhang S, Tan Y. Single-spot two-dimensional displacement measurement based on self-mixing interferometry. Optica. 2017;4(7). doi: 10.1364/optica.4.000729.
33. Zhao Y, Zhu D, Chen Y, Tu Y, Bi T, Zhao Y, et al. All-fiber self-mixing laser Doppler velocimetry with much less than 0.1 pW optical feedback based on adjustable gain. Optics Letters. 2020;45(13):3565-8. doi: 10.1364/ol.397819.

34. Otsuka K, Ohtomo T, Makino H, Sudo S, Ko JY. Net motion of an ensemble of many Brownian particles captured with a self-mixing laser. Applied Physics Letters. 2009;94(24):3. doi: 10.1063/1.3156826.
35. Mowla A, Bertling K, Wilson SJ, Rakic AD. Dual-Modality Confocal Laser Feedback Tomography for Highly Scattering Medium. IEEE Sensors Journal. 2019;19(15):6134-40. doi: 10.1109/jsen.2019.2910122.
36. Gouaux F, Servagent N, Bosch T. Absolute distance measurement with an optical feedback interferometer. Applied Optics. 1998;37(28):6684-9. doi: 10.1364/ao.37.006684.
37. Lu C, Liu G, Liu B, Chen F, Gan Y. Absolute distance measurement system with micron-grade measurement uncertainty and 24 m range using frequency scanning interferometry with compensation of environmental vibration. Opt Express. 2016;24(26):30215-24. doi: 10.1364/OE.24.030215.
38. Hugon O, Lacot E, Stoeckel F. Submicrometric displacement and vibration measurement using optical feedback in a fiber laser. Fiber and Integrated Optics. 2003;22(5):283-8. doi: 10.1080/01468030390221696.
39. Xu Z, Li J, Zhang S, Tan Y, Zhang X, Lin X, et al. Remote eavesdropping at 200 meters distance based on laser feedback interferometry with single-photon sensitivity. Optics and Lasers in Engineering. 2021;141. doi: 10.1016/j.optlaseng.2021.106562.
40. Glombitza U, Brinkmeyer E. COHERENT FREQUENCY-DOMAIN REFLECTOMETRY FOR CHARACTERIZATION OF SINGLE-MODE INTEGRATED-OPTICAL WAVE-GUIDES. Journal of Lightwave Technology. 1993;11(8):1377-84. doi: 10.1109/50.254098.
41. Moore ED, McLeod RR. Correction of sampling errors due to laser tuning rate fluctuations in swept-wavelength interferometry. Optics Express. 2008;16(17):13139-49. doi: 10.1364/oe.16.013139.
42. Jacquin O, Lacot E, Felix C, Hugon O. Laser optical feedback imaging insensitive to parasitic optical feedback. Applied Optics. 2007;46(27):6779-82. doi: 10.1364/ao.46.006779.
43. Zhang Y, Hines AS, Valdes G, Guzman F. Investigation and Mitigation of Noise Contributions in a Compact Heterodyne Interferometer. Sensors (Basel). 2021;21(17). doi: 10.3390/s21175788.
44. Zhang X, Pouls J, Wu MC. Laser frequency sweep linearization by iterative learning pre-distortion for FMCW LiDAR. Opt Express. 2019;27(7):9965-74. doi: 10.1364/OE.27.009965.
45. Zhao Y, Wang C, Zhao Y, Zhu D, Lu L. An all-fiber self-mixing range finder with tunable fiber ring cavity laser source. Journal of Lightwave Technology. 2020:1-. doi: 10.1109/jlt.2020.3043331.
46. Lacot E, Hugon O. Frequency-shifted optical feedback in a pumping laser diode dynamically amplified by a microchip laser. Applied Optics. 2004;43(25):4915-21. doi: 10.1364/ao.43.004915.

Figures

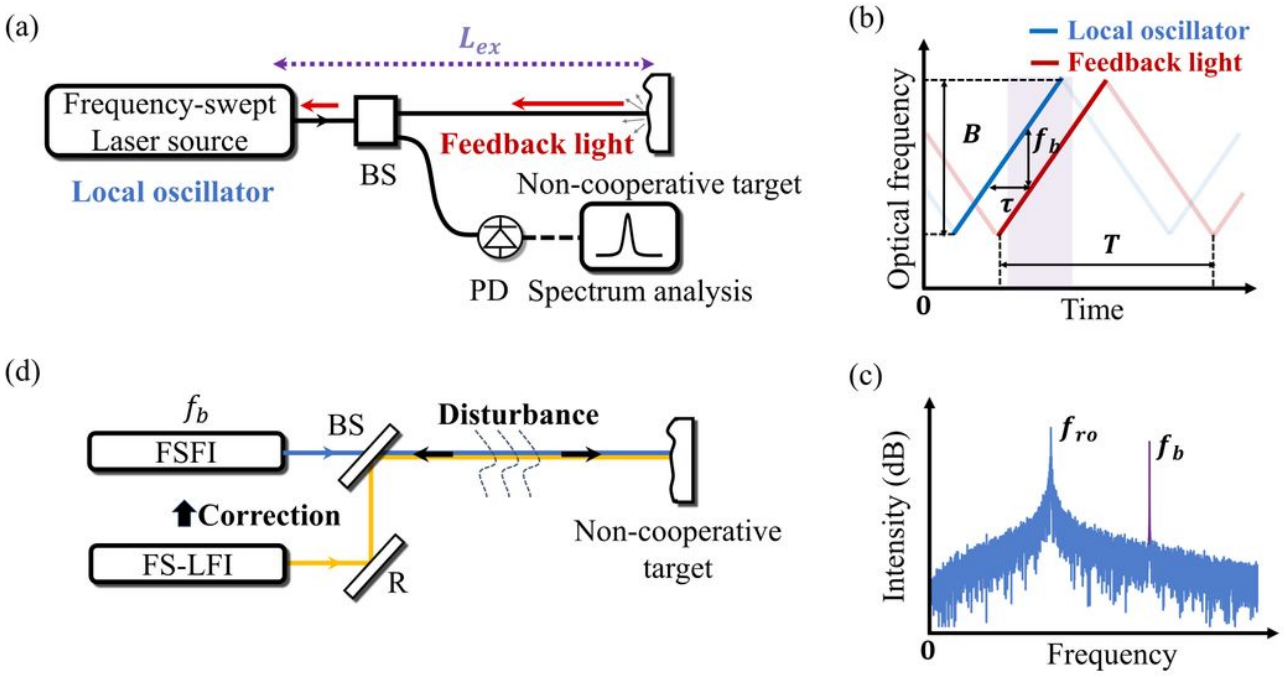

Figure 1

(a) Principle diagram of the FSFI ranging system. BS, beam splitter; PD, photodetector; R, reflector. (b) The waveform of the swept optical frequency. (c) The intensity spectrum of the laser output. (d) Configuration of the FSFI ranging system with optical path length drift compensation.

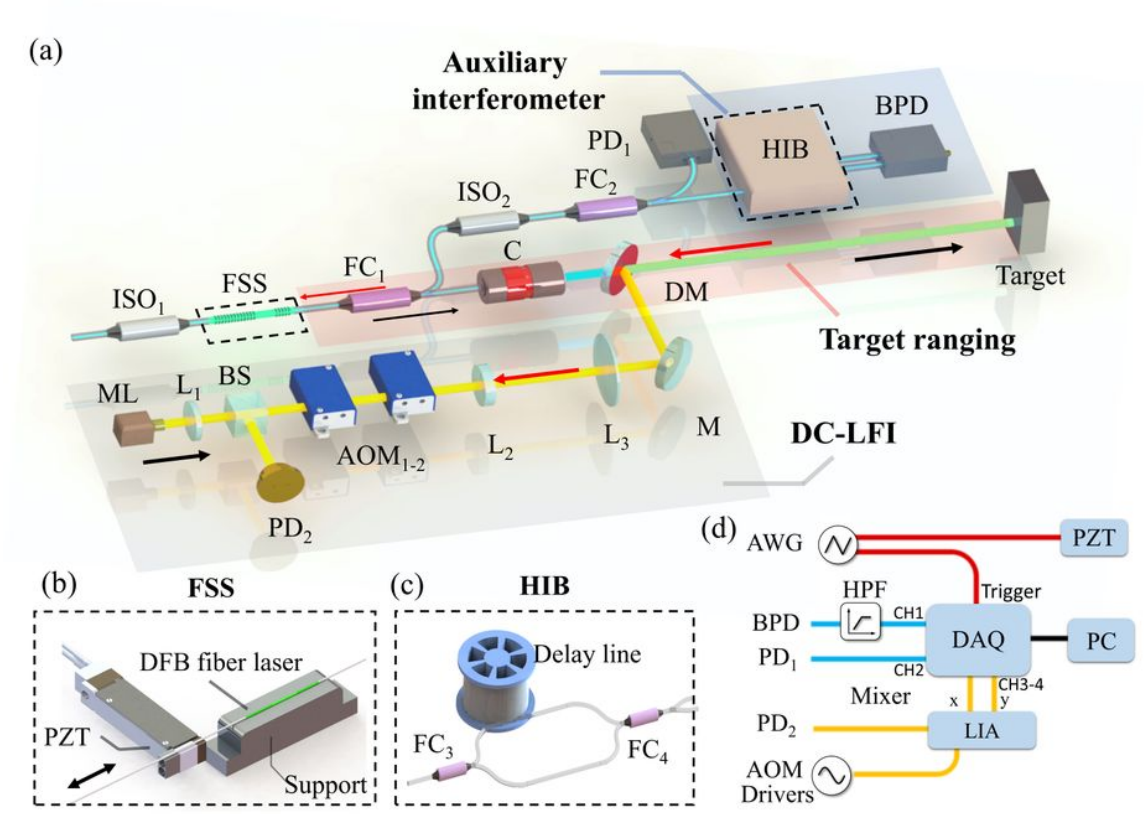

Figure 2

Schematic diagram of the proposed FSFI ranging system with OPL drift compensation. (a) Optical design. FSS, frequency-swept source; ISO, optical isolator; FC, fiber coupler; PD, photodetector; HIB, heat insulation box; BPD, balanced photodetector; C, collimator; DM dichroic mirror; ML, microchip laser; L, lens; BS, beam splitter; AOM, acoustic-optic modulator; M, reflective mirror; The pink region marks the ranging module and illustrates the optical path to be detected. The blue and gray marked region stands for the auxiliary interferometer and frequency-shifted interferometer. (b) Schematic of the FSS; PZT, piezoelectric ceramic actuator. (c) Schematic of the Mach-Zehnder-type fiber interferometer in HIB. A piece of G652.D fiber is used as the delay line. (d) Schematic of the data acquisition. AWG, arbitrary waveform generator; DAQ, data acquisition card; LIA, lock-in amplifier; PC, computer

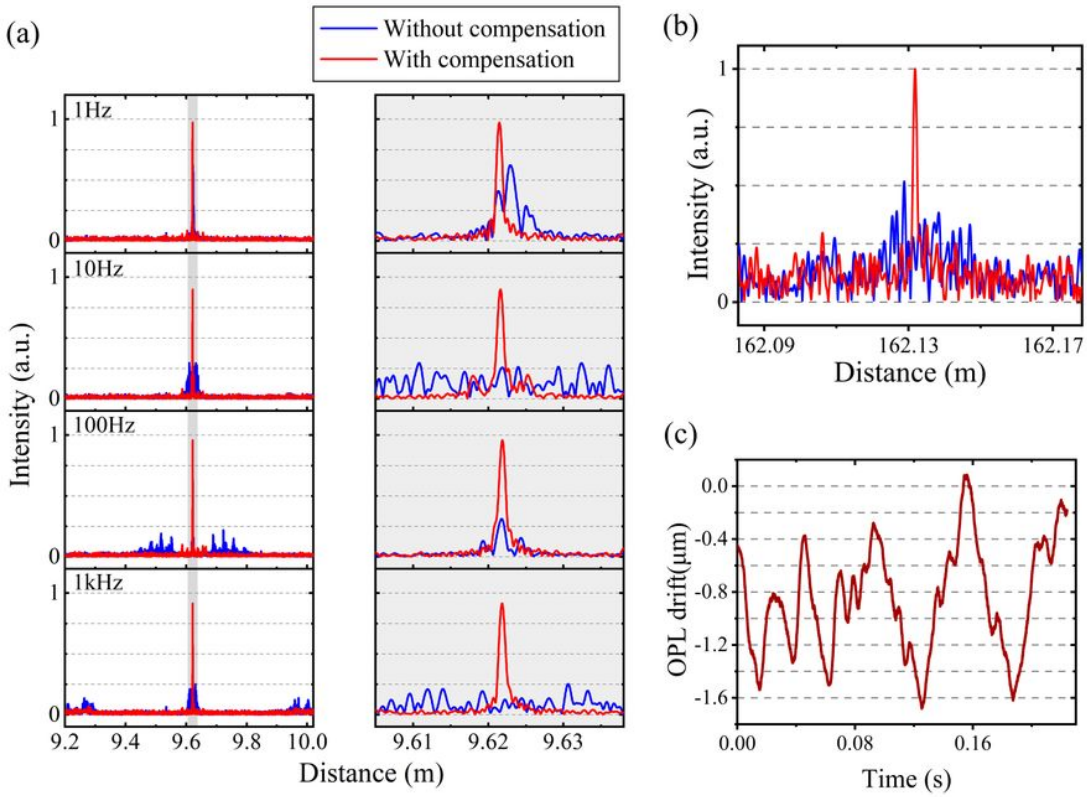

Figure 3

Performance of the DC-LFI-based compensation method. (a) Ranging results of an aluminum sheet vibrating at 1Hz, 10Hz, 100Hz, and 1kHz with or without compensation. The right column is the zoomed details of the gray-marked parts respectively in the left column. (b) Ranging results with 162m stand-off distance (c) The OPL drift recorded by DC-LFI during ranging corresponding to (b).

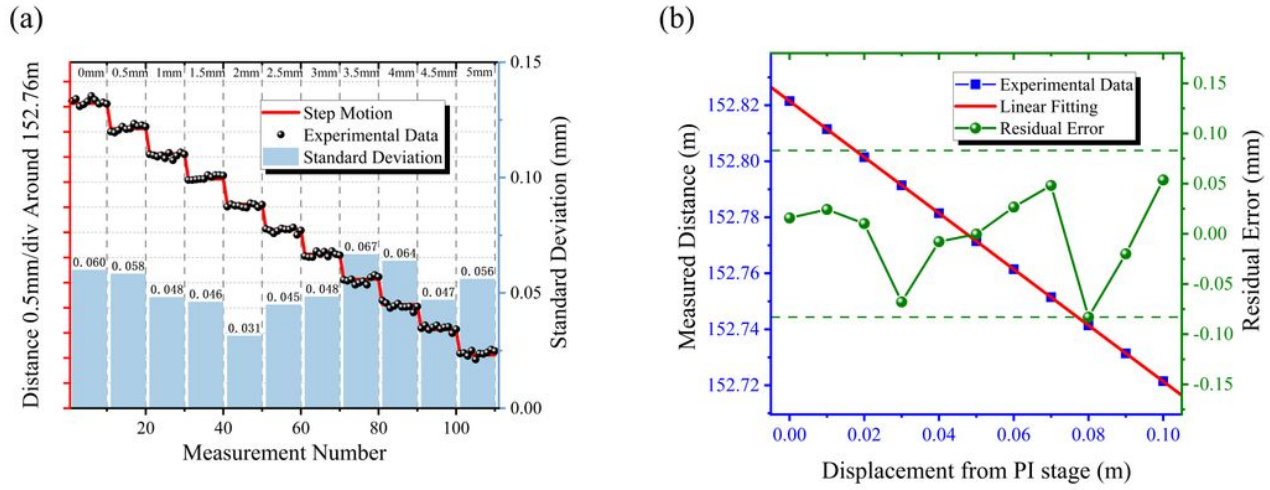

Figure 4

Results of the precision tests. (a) The standard deviation of 10 measurements with different stand-off distances around 152.76m. The target is an aluminum sheet. (b) The linearity-test results of the system.

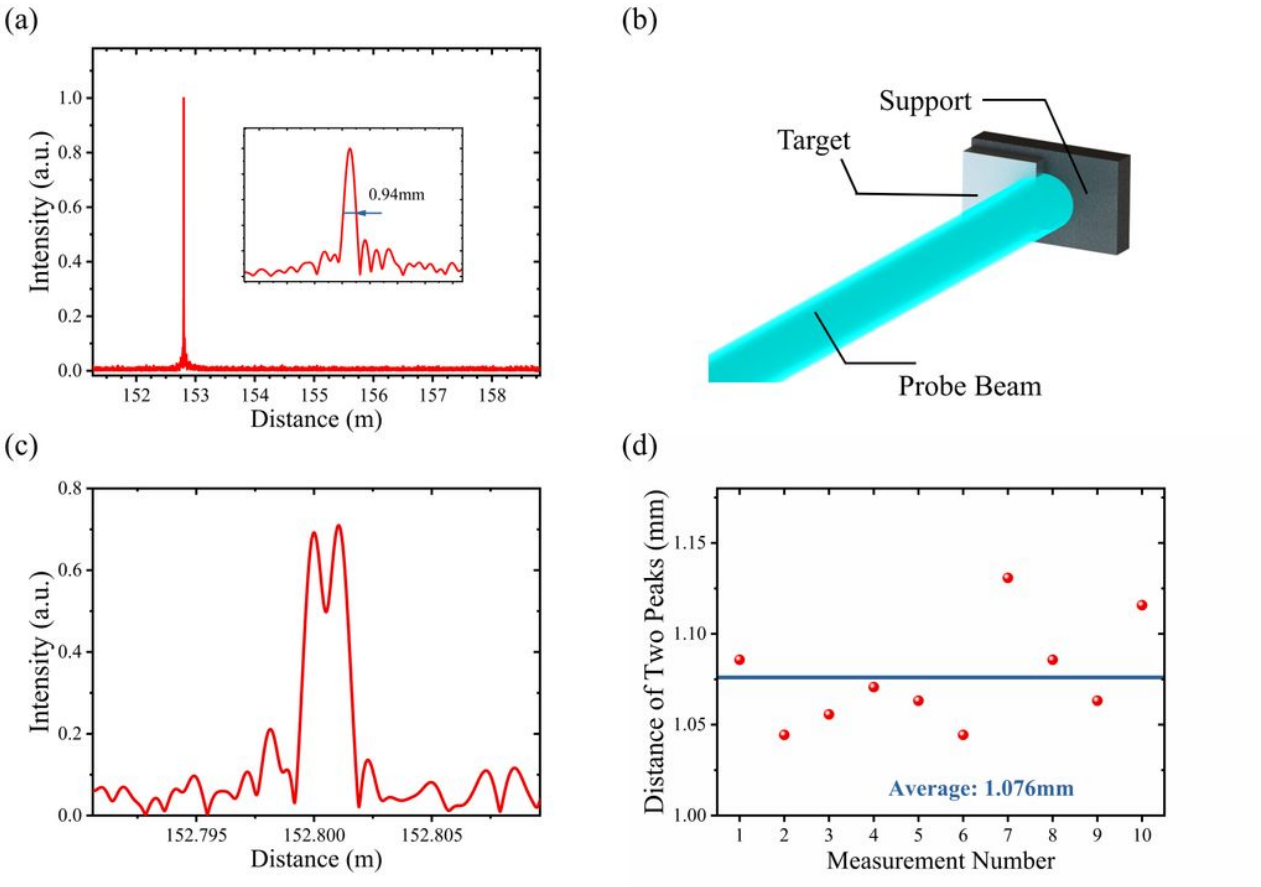

Figure 5

Results of resolution tests. (a) Ranging results of an aluminum sheet 152m away from the system. Inset: zoomed details of the peak. (b) Schematic diagram of the ranging targets in resolution experiments. (c) Ranging results with two targets (d) The gap measured in 10 times repeats.

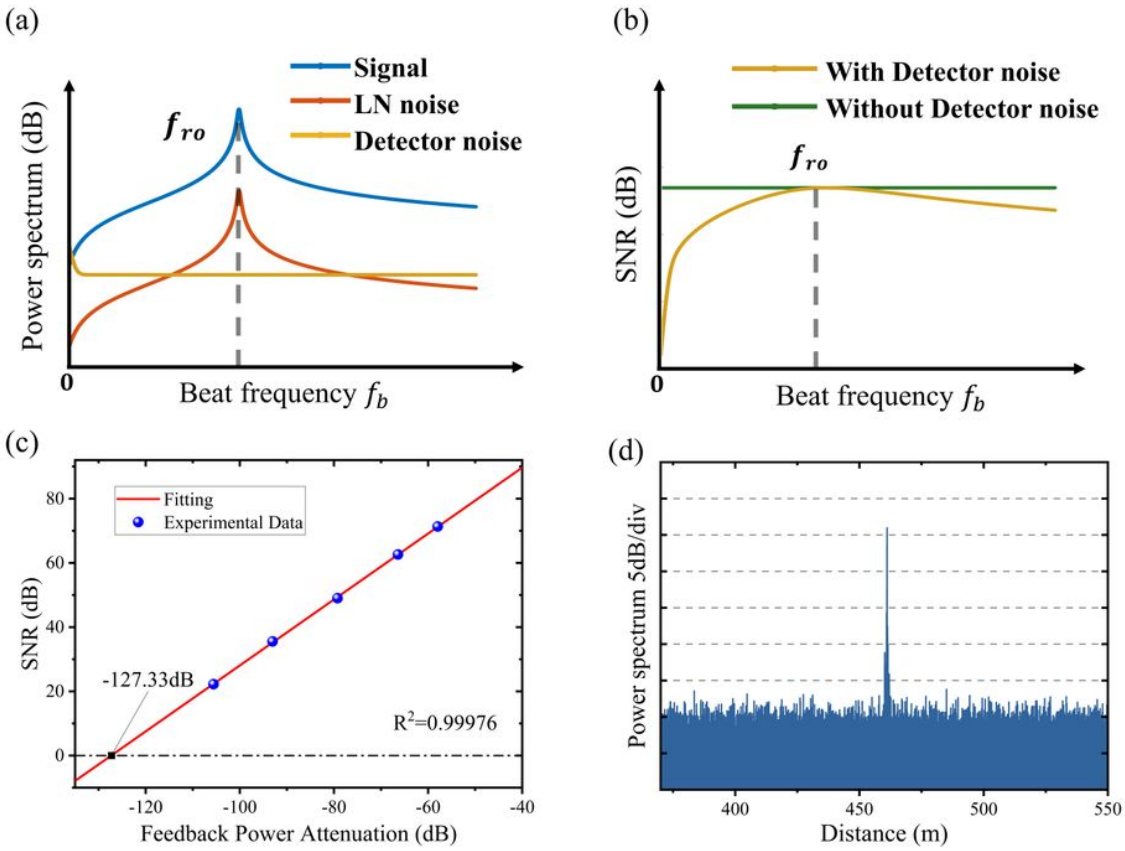

Figure 6

SNR and Detection limits of the system. (a) The normalized power spectra verse the beat frequency fb. (b) The SNR with and without the PD noise. (c) SNR verse various feedback power attenuation. Red solid line: linear fitting result. Black dash-dotted line: SNR=1. (d) Ranging results with 460m stand-off distance.

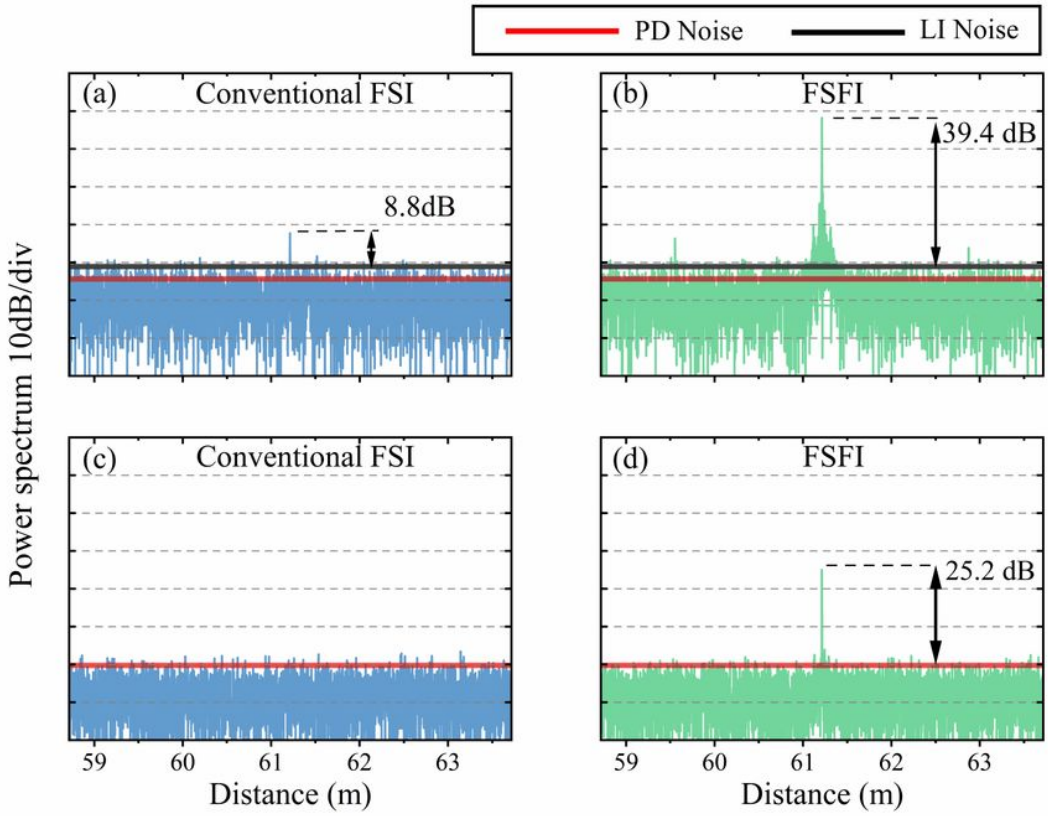

Figure 7

Power spectra of the conventional LFI and FSFI in ranging. PD noise, photodetector noise. LI noise, laser intensity noise. (a)-(b) LI noise is stronger than PD noise. (c)-(d) PD noise is stronger than LI noise. (a) and (c) are from the conventional LFI-based ranging system. (b) and (d) are from the FSFI-based ranging system.

Supplementary Files

This is a list of supplementary files associated with this preprint. Click to download.

- Supplementalmaterial.docx